Biochemical and Biophysical Research Communications 426 (2012) 585–589

Contents lists available at SciVerse ScienceDirect

Biochemical and Biophysical Research Communications

journal homepage: www.elsevier.com/locate/ybbrc

Modulation of membrane rigidity by the human vesicle trafficking proteins Sar1A and Sar1B

Andrew F. Loftus [a], Vivian L. Hsieh [a], Raghuveer Parthasarathy [b,c,*]

[a] Department of Chemistry, 1274 University of Oregon, Eugene, OR 97403-1274, USA
[b] Department of Physics, 1274 University of Oregon, Eugene, OR 97403-1274, USA
[c] Materials Science Institute, 1274 University of Oregon, Eugene, OR 97403-1274, USA

ARTICLE INFO

Article history:
Received 21 August 2012
Available online 4 September 2012

Keywords:
Lipid bilayer
Vesicle trafficking
Optical traps
Membrane rigidity
Sar1

ABSTRACT

The sculpting of membranes into highly curved vesicles is central to intracellular cargo trafficking, yet the mechanical activities of trafficking proteins remain poorly understood. Using an optical trap based assay that measures *in vitro* membrane response to imposed deformations, we examined the behavior of the two human paralogs of Sar1, a key component of the COPII family of vesicle coat proteins. Like their yeast counterpart, the human Sar1 proteins can lower the mechanical rigidity of the membranes to which they bind. Unlike the yeast Sar1, the rigidity is not a monotonically decreasing function of concentration. At high concentrations, we find increased bending rigidity and decreased protein mobility. These features imply a model in which protein clustering governs membrane mechanical properties.

1. Introduction

The trafficking of cargo from membranous organelles involves dramatic manipulations of membrane shape. Trafficking proteins must bind to and bend membranes, creating highly curved forms that are subsequently constricted at a neck, pinched off, and ferried to their destinations along with encapsulated cargo. Though a great deal is known about the molecular structures and biochemical properties of trafficking proteins, and about the physical principles relevant for curvature generation [1–4], the mechanisms by which specific trafficking systems harness particular forces and material properties remain largely mysterious.

We recently showed that the trafficking protein Sar1p, a key component of the coat protein II (COPII) system in yeast, lowers the bending rigidity of the lipid bilayer to which it binds, providing the first reported example of a trafficking protein that "softens" its target membrane [5]. Sar1p is the only member of the COPII vesicle coat that binds directly to the lipid bilayer, which it does via an N-terminal amphipathic alpha helix that is exposed when the protein is in its GTP-bound conformation [6–8]. The other COPII proteins bind to Sar1 or to each other, assembling the vesicle coat and recruiting cargo [9]. Sar1p's ability to lower membrane rigidity suggests a model in which membrane-bound Sar1-GTP lowers the energetic cost for the other COPII proteins, especially the polyhedra-forming Sec13 and Sec31 [10], to generate curvature.

In mammals there are two Sar1 paralogs, denoted Sar1A and Sar1B in humans, which share an 89% amino acid identity with each other. All three Sar1s have similar secondary structures [4,11,12] and possess an N-terminal amphipathic alpha helix (Fig. 1A). Interestingly, rare fat adsorption disorders involving transport of large lipid capsules are associated with defects in Sar1B but not Sar1A [13], and Sar1B has been suspected to generate larger vesicles than Sar1A [14], observations that may point to differences in the modulation of bending rigidity between the two human proteins. It has remained unknown, however, whether the human Sar1 proteins lower membrane rigidity at all, and if so, whether they do so in a manner that is similar to that of the yeast Sar1p. We therefore measured the rigidity of lipid bilayer membranes as a function of Sar1A or Sar1B concentration using the assay previously applied to Sar1p, described in detail in Ref. [5].

2. Materials and methods

As in [5], lipid membranes were composed of the "Major Mix" mixture [5], similar in composition to the endoplasmic reticulum membrane, modified to include fluorescent probes and biotinylated lipids: 51.5 mol% DOPC (1,2-dioleoyl-sn-glycero-3-phosphocholine), 23.0 mol% DOPE (1,2-di-(9Z-octadecenoyl)-sn-glycero-3-phosphoethanolamine), 11.0 mol% PI (L-α-phosphatidylinositol, from Soy), 8.0 mol% DOPS (1,2-diacyl-sn-glycero-3-phosphoserine), 5.0 mol% DOPA (1,2-di-(9Z-octadecenoyl)-sn-glycero-3-phosphate), 0.5 mol% Texas Red DHPE (Texas Red 1,2-dihexadecanoyl-sn-glycero-3-phosphoethanolamine), and 1.0 mol% biotinyl-cap-PE

* Corresponding author at: Department of Physics, Materials Science Institute, 1274 University of Oregon, Eugene, OR 97403-1274, USA. Fax: +1 541 346 5861.
E-mail address: raghu@uoregon.edu (R. Parthasarathy).

0006-291X/$ - see front matter © 2012 Elsevier Inc. All rights reserved.
http://dx.doi.org/10.1016/j.bbrc.2012.08.131

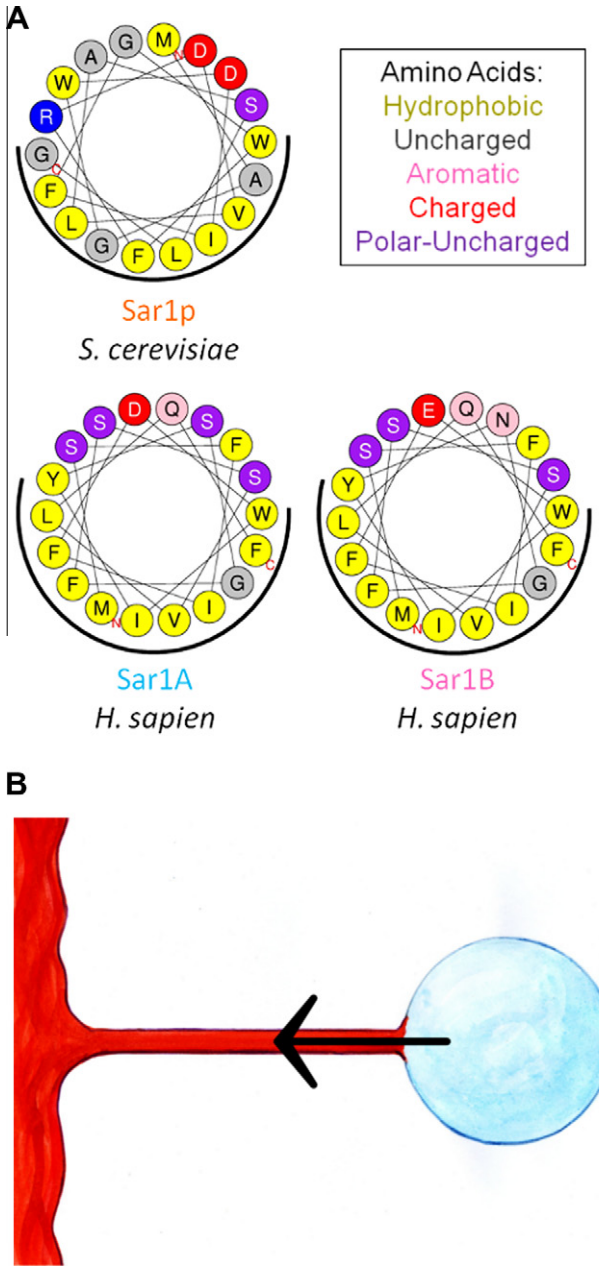

Fig. 1. (A) Helical wheel plots of the N-terminal amino acids of Sar1 proteins. Each Sar1 has a distinctive hydrophobic hull (black arc) with charged residues on the opposite face, enabling association with lipid bilayers. (B) Schematic illustration of the tether-pulling rigidity assay. Lipid bilayers are incubated with Sar1 proteins and membrane-binding microspheres. Pulling a microsphere with an optical trap yields a cylindrical membrane tether. Turning off the trap, the tether retracts (arrow) to lower the mechanical energy associated with its high curvature, pulling the microsphere along with it. Measurement of the tether radius and retraction force reveals the bending rigidity of the membrane.

(1,2-dihexadecanoyl-sn-glycero-3-phosphoethanolamine-*N*-(cap biotinyl)).

Sar1 was expressed and purified using protocols similar to those in [15]. Protein expression was performed with a PTY40 expression vector (a pGEX-2T backbone (GE Healthcare) with inserted GST-Sar1 strain RSB245410 (Sar1p), RSB3771 (Sar1A) or RSB3772 (Sar1B) (Schekman Group, UC Berkeley) in BL21 bacterial expression cells.

Nucleotide binding, membrane tether pulling, analysis of rigidity, and associated procedures were performed as discussed in [5]. Multilayered membrane stacks were formed by depositing approximately 5 μg of lipids dissolved in chloroform onto chambered glass coverslips. The solvent was evaporated in a vacuum desiccator for 5 m after which the lipids were hydrated with 0.2 ml HKM buffer (20 mM Hepes–KOH, pH 6.8, 160 mM potassium acetate, 1 mM $MgCl_2$), yielding multilayered membrane stacks. Bovine serum albumin (BSA) was adsorbed to the glass prior to lipid deposition in order to prevent van der Waals adhesion of microspheres; BSA was incubated at 1 mg/ml for several hours, followed by repeated washing. Sar1A, Sar1B or Sar1p, 100 μM GMPPNP (Sigma–Aldrich) and 4 mM EDTA were incubated together in a vial for 5 m, after which they were added to the chamber containing membranes and buffer. Approximately five minutes after the addition of protein, a suspension of 4.8 μm diameter streptavidin-coated silica microspheres (Bangs Laboratories) were added to the chamber. The microspheres gravitationally settled and bound to the membranes. Microspheres were trapped with a home-built optical trap setup using a 671-nm, 120-mW diode laser (model No. RS71-100PS; Meshtel, AKA Intelite, Genoa, NV). Tethers were pulled from thick multilayers as in Ref. [5], roughly parallel to the coverslip plane to facilitate tether imaging. Microsphere images were captured with bright-field microscopy using a Model No. pco.1200 camera (Cooke, Romulus, MI) at 100 frames per second.

Particle positions were determined using home-built tracking software. Hough transformation of ring-like brightfield particle images yielded peaks whose centers were determined by nonlinear fitting of two-dimensional Gaussian functions. Tracking test particles stuck to glass coverslips, with the same exposure and illumination settings, shows a localization precision of 5 nm (0.02 px), as would be expected [16] for images with a signal-to-noise ratio of 100. The drag coefficient, b, is determined from velocity fluctuations for each tether independently following the general approach described by Sainis et al. [17]. The uncertainty in b due to tracking precision is approximately 1%, and so is negligible compared to the statistical variability of tether data. Alternatively localizing particles by fitting ring-like particle images directly using a radial-symmetry-based fitting [16], without the intermediate step of Hough transformation, yields indistinguishable results.

Fluorescence images of membrane tethers were captured with an ORCA-ER charge-coupled device camera (Hamamatsu, Hamamatsu City, Japan). Tether radii were determined as in Ref. [5].

Sar1 proteins were prepared and incubated with Major Mix membranes in the same manner as described above, but with the non-hydrolyzable nucleotide GMPPNP replaced by the fluorescent BODIPY FL GTP-γ-S (BD-GTP-γ-S, Life Technologies) to visualize the Sar1 bound to membranes. Gentle washing with protein-free HKM buffer was performed to remove excess BD-GTP-γ-S and unbound protein. Fluorescence images were taken of both Sar1- BD-GTP-γ-S and Texas Red-DHPE (fluorescent lipid) with the ORCA-ER CCD camera. Intensity values and background subtraction were performed using in-house software written in MATLAB (MATHworks).

Protein and lipid mobilities were measured by examining fluorescence recovery after photobleaching (FRAP) [18]. For each measurement fluorescent probes were bleached for 2–3 s with a 473 nm, 50 mW diode laser (DHOM Model number: DHL25A, Ultralasers) focused to a spot. Images were acquired at discrete time points after bleaching and analyzed to determine the diffusion coefficients by modeling fluorescence recovery as a two-dimensional random walk, as described elsewhere [19]. In brief, we determine the diffusion coefficient that generates the best fit match between a time-evolved initial image and a measured final image, an approach that requires no assumptions about the size or shape of the bleached spot.

3. Results

In Fig. 2A, we plot κ_0 normalized by κ_{lipid}, the membrane rigidity in the absence of protein, as a function of the solution concentration of Sar1 ([Sar1]) for each of the Sar1 proteins examined. The Sar1p data, previously reported in Ref. [5], showed a monotonic decrease in membrane rigidity as a function of protein concentration. At [Sar1p] $\approx$ 20 μM and greater, Sar1p incubation results in dramatic shape fluctuations and disintegration of the membrane as shown in Fig. 2B and C. At these concentrations, tether retraction experiments were impossible, and the observed dynamics imply a very low rigidity, comparable to the ambient thermal energy, as indicated by the box in Fig. 2A.

At low concentrations, the human proteins Sar1A and Sar1B also lower membrane rigidity, though by a lesser amount than Sar1p (Fig. 2A). Strikingly, the rigidity of the membrane increases with concentration above 10 μM. Qualitatively, this high rigidity is evident from the integrity of tethers and membrane edges (Fig. 2D and E). Quantitatively, tether retraction measurements reveal the increase in κ_0, which is more pronounced for Sar1A than Sar1B (Fig. 2A). We also plot in Fig. 2A and B curves from a model that provides a possible functional form for the concentration dependence of κ_0, discussed later in the text.

To determine whether the different rigidities simply mirror differences in membrane-bound concentration among the various proteins, we determined the binding affinities of the Sar1s. Experiments using reactive fluorophores conjugated to primary amines on the proteins themselves yielded highly variable degrees of labeling. We therefore used a fluorescent non-hydrolyzable nucleotide, BODIPY FL GTP-γ-S, as an indicator of protein abundance. In all experiments, the BODIPY fluorescence intensity (I_{Sar1}) and the fluorescence intensity of Texas Red lipid probes (I_{lipid}) are measured following washing to remove unbound proteins and nucleotide. Normalizing the background-subtracted I_{Sar1} by I_{lipid} (to account for small variations in illumination intensity) provides the normalized fluorescence intensity plotted in Fig. 3. The data show similar two-dimensional protein abundances for all the Sar1 proteins. A fit to a Langmuir isotherm gives a binding constant of $K_D = 10.5 \pm 3.1$ μM, with no significant difference among the Sar1 types. This suggests that differential binding affinities of the protein to the membrane are not the cause of differences in the modulation of the membrane rigidity.

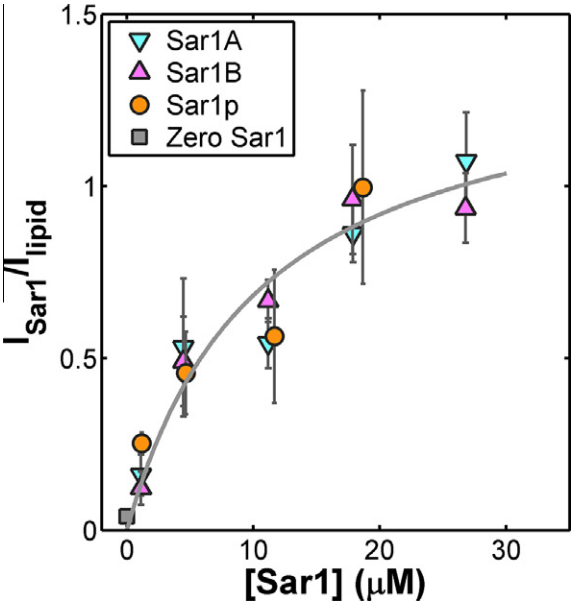

Fig. 3. Normalized intensity of fluorescent nucleotides, providing a measure of membrane-bound protein concentration, as a function of the solution concentration of Sar1. The binding behaviors of all three proteins to the lipid membrane are similar. A Langmuir isotherm fit to all the data (solid curve) gives $K_D = 10.5 \pm 3.1$ μM.

Hypothesizing that differences in rigidity may correlate with differences in in-plane mobility, we measured the diffusion (D_{lipid}) and membrane-bound Sar1 proteins (D_{Sar1}) by performing fluorescence recovery after photobleaching (FRAP) experiments [20–22] on fluorescent lipid probes and fluorescent nucleotides (see Experimental Methods, provided as Supporting Information). We show in Fig. 4A and B examples of photobleached spots and their recoveries for both the lipid and protein probes. Throughout the full range of concentrations examined, lipids and proteins are all mobile, implying that none of the Sar1 proteins form a rigid scaffold. Quantification of the diffusion coefficients reveals differences in the behaviors of the yeast and human Sar1s. As a function of concentration, D_{Sar1} is roughly constant for Sar1p, while it decreases significantly for the human proteins (Fig. 4C). The low mobility

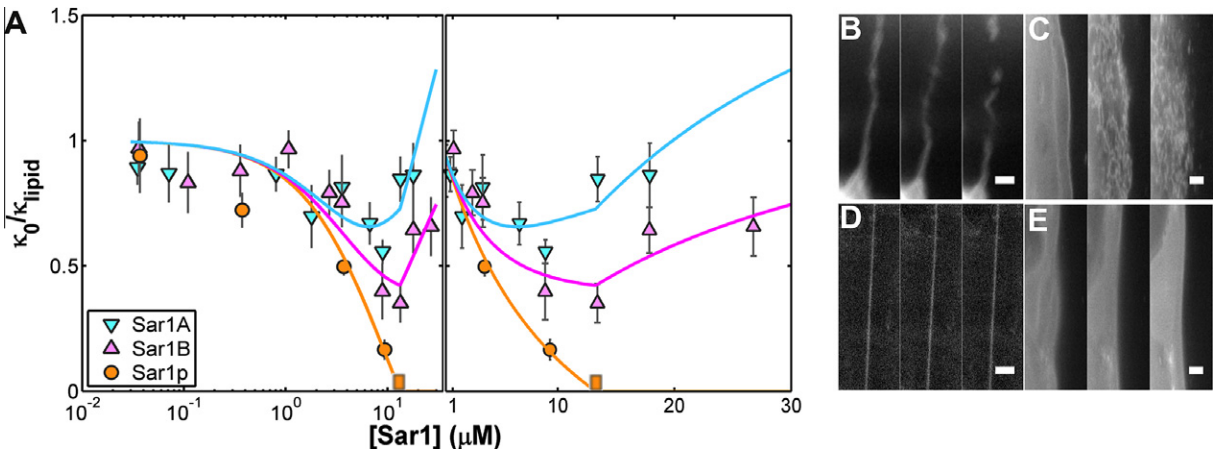

Fig. 2. (A) Membrane rigidity as a function of Sar1 concentrations. Data for membranes with Sar1p (orange circles) were reported previously [5]. The orange box is shown at the concentration at which Sar1p induced membrane disintegration, implying near-zero rigidity. Lines indicate fits to the model discussed in the text. The left and right panels show the same data using logarithmic and linear concentration axes, respectively. (B, C) Fluorescence images of Texas Red DHPE labeling lipid membranes in the presence of 20 μM Sar1p, depicting (B) a tether and (C) an unperturbed multilayer region of membrane. The three images in B and C are each separated in time by 15 s. (D, E) Lipid fluorescence images in the presence of 20 μM Sar1B, depicting (D) a tether and (E) an unperturbed multilayer region of membrane. The three images in D and E are each separated in time by 1 min. Scale Bars = 5 μm. (For interpretation of the references to color in this figure legend, the reader is referred to the web version of this article.)

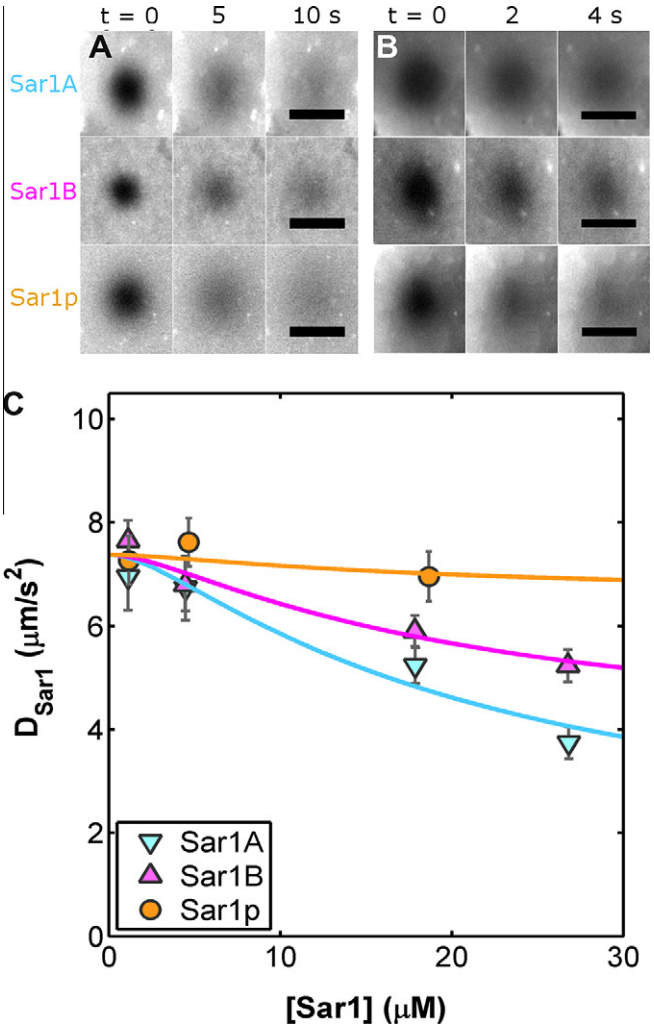

Fig. 4. (A) Time-lapse fluorescence images of Texas Red DHPE during FRAP experiments probing membrane mobility. The three rows correspond to membranes incubated with Sar1A, Sar1B, and Sar1p. (B) Time-lapse fluorescence images of BODIPY FL GTP-γS during FRAP experiments probing the mobility of membrane-bound protein. (C) Protein diffusion coefficients as a function of incubation concentration for the various Sar1 proteins. Solid lines are fits to the model discussed in the text. Scale bars in (A) and (B) are 25 μm.

at high concentration is more pronounced for Sar1A than Sar1B (Fig. 4C). This trend is also reflected in the lipid diffusion coefficients. At [Sar1] ≈ 20 μM, D_{lipid} with bound Sar1p is 5.1 ± 1.0 μm²/s, identical within uncertainties to the value with no protein, 5.6 ± 0.6 μm²/s. In contrast, D_{lipid} = 2.7 ± 0.5 μm/s² for Sar1A and 3.0 ± 0.4 μm/s² for Sar1B.

4. Discussion

The rigidity, mobility, and binding affinity measurements described above suggest that the human Sar1 proteins, unlike yeast Sar1, may interact with one another at the membrane, forming assemblies that are stiffer and less mobile than membranes solely bound by protein monomers. While an infinite number of models could be concocted to mimic these observations, our ignorance of the structural mechanisms of potential inter-protein interactions motivates a minimalist approach of constructing the simplest possible non-trivial model, asking whether the functional form of the rigidity and mobility it predicts are mirrored by the data, and allowing only a small number of free parameters. Our simple model assumes that all Sar1 proteins lower membrane rigidity by an amount proportional to their two-dimensional concentration, that Sar1A and Sar1B proteins have a weak affinity for dimerization, and that rigidity and mobility induced by Sar1A and Sar1B are proportional to the dimer concentration. Of course, higher order dependences of rigidity and mobility on concentration, as well as higher order oligomerization, are possible; invoking them would introduce additional parameters.

We decompose the membrane bending rigidity (κ) into the sum of the rigidities induced by individual proteins (κ_s) and by dimers (κ_{dimer}):

$$\kappa = \kappa_S + \kappa_{dimer} \tag{1}$$

Neglecting dimerization, we propose that Sar1 proteins monotonically lower κ_s, the simplest form for which is a linear decrease in rigidity as a function of membrane-bound protein concentration:

$$\kappa_s = \kappa_{lipid}(1 - \alpha^{-1}c), \tag{2}$$

where κ_{lipid} is the rigidity in the absence of protein, c is the two-dimensional concentration of the protein at the membrane normalized by the maximal protein density, and α is the critical concentration at which the membrane reaches zero rigidity. By construction, $\alpha \leqslant 1$; the empirically determined value of this parameter is discussed below. The rigidity κ_s is constrained to be non-negative.

The two-dimensional concentration, c, as a function of the solution concentration of protein, [Sar1], is provided by the binding data shown in Fig. 3, which can be fit to a Langmuir isotherm:

$$c = \frac{[\text{Sar1}]}{K_D + [\text{Sar1}]}. \tag{3}$$

The equilibrium between membrane-bound monomers (p) and dimers (p–p), written as $p + p \leftrightarrow p$–p, implies that $c_d = K_2 c_m^2$, where c_d and c_m are the two-dimensional concentrations of dimers and monomers, respectively, and K_2 is the binding constant. For weak binding, i.e. to lowest order in $K_2 c$, $c_d \approx K_2 c^2$, providing a simple relationship between dimer density and overall membrane-bound concentration.

We propose that dimers increase rigidity, since they correspond to fixed spatial arrangements of membrane-bound proteins, and that the dimer-induced rigidity is directly proportional to c_d, from which

$$K_{dimer} = K_p c^2, \tag{4}$$

where the parameter κ_p characterizes the dimer stiffness and binding affinity. (In other words, $\kappa_{dimer} = Bc_d$ for some stiffness parameter B, which can be written $\kappa_{dimer} = BK_2c^2$. Since K_2 and B are not separately measurable, we subsume them into a single parameter, κ_p).

Eqs. (1)–(4) characterize our model. The parameters α, K_D, and κ_p could in principle be different for all the proteins, but in practice are highly constrained by data. As noted above, the membrane-binding affinity is K_D = 10.5 ± 3.1 μM for all the proteins. The rigidity in the absence of protein, κ_{lipid}, is directly measured (alternatively, κ_{lipid} can be treated as a fit parameter; this is discussed in the Supporting Information). We assume that Sar1p does not dimerize, and so its κ_p = 0, allowing its rigidity data (Fig. 2A) to be fit with only one free parameter, α, yielding α = 0.56 ± 0.02. Using this same α for the human Sar1 proteins (i.e. treating the membrane softening, not related to dimerization, as being the same for all Sar1s), we can fit the Sar1A and Sar1B rigidity data with only one free parameter, κ_p, for each protein species. We find good agreement between the data and the form of κ predicted by the model (Fig. 2A, solid curves), and find for Sar1A, $\kappa_{p,Sar1A}/\kappa_{lipid}$ = 2.3 ± 0.44, and for Sar1B, $\kappa_{p,Sar1B}/\kappa_{lipid}$ = 1.4 ± 0.38,

quantifying the greater rigidity of Sar1A relative to Sar1B observed in tether-pulling experiments.

We can similarly ask whether the protein diffusion coefficient (D_p) decreases proportionally with dimer concentration:

$$D_p = D_0(1 - dc^2) \quad (5)$$

where D_0 is the diffusion coefficient at [Sar1] → 0 and d is a dimensionless parameter. Fitting the data shown in Fig. 4C yields $D_0 = 7.4 \pm 0.2$ μm/s^2 for all the proteins. For Sar1A, we find $d_{Sar1A} = 0.87 \pm 0.13$ and for Sar1B $d_{Sar1B} = 0.54 \pm 0.08$. The Sar1p data show $d_{Sar1p} = 0.12 \pm 0.11$, consistent with negligible dimerization.

Notably, the ratio of the mobility reductions for the human proteins $d_{Sar1A}/d_{Sar1B} = 1.6 \pm 0.3$, identical within uncertainties to the ratio of the relative rigidity parameters: $\kappa_{p,Sar1A}/\kappa_{p,Sar1B} = 1.6 \pm 0.6$. The similarity of these ratios for two independently measured and physically distinct physical properties further supports the proposed model, in which the existence of dimers of the human Sar1 proteins is the shared determinant of increased stiffening and lower mobility. We stress, however, that the validity of the model is separate from the main experimental conclusions of this work, that the human Sar1 proteins nonmonotonically alter membrane rigidity as a function of concentration. We believe the model provides a useful framework for envisioning the possible molecular mechanisms underlying our observations, and hope that this may spur studies of weak interactions among membrane-associated proteins that may be feasible using recently developed resonance energy transfer or correlation spectroscopy techniques [23].

The mechanics of membrane deformation are of importance to a wide variety of cellular processes. Though the imposition of specific curvatures by scaffold-like molecules, for example proteins with crescent-shaped BAR domains [24,25] or lipids with particular spontaneous curvatures [26,27], have generated a great deal of interest in recent years, situations in which proteins generally alter membrane stiffness remain underexplored. We have measured the rigidity of membranes bound by the human COPII proteins Sar1A and Sar1B. Like the yeast Sar1 protein, the human paralogs are capable of lowering the membrane bending modulus. Unlike the yeast protein, however, the human Sar1s show increased membrane rigidity at high concentrations, concurrent with a reduction in mobility, with the concentration dependence of both of these behaviors implying the existence of protein-protein interactions. Our quantification of greater rigidity from membrane-bound Sar1A than from Sar1B may help explain phenomenological observations of different transport-related disorders [13], and different trafficking vesicle morphologies [14] induced by these two proteins. In each of these cases, Sar1B is associated with larger structures, consistent, all other things being equal, with a lower rigidity induced by this protein compared to Sar1A. More generally, the rigidity values we have measured, as well as the parameters output by a simple model of dimer-induced physical changes, should form key ingredients of potential mechanochemical models of vesicle trafficking, since rigidity determines the energetic requirements of curvature generation [1–3]. Such models are beginning to exist for other vesicular systems [28], and we hope to encourage their formulation for the COPII transport machinery.

Acknowledgments

We thank Karen Kallio and Jim Remington for assistance with protein expression and Bob Lesch and Randy Schekman for providing plasmids for Sar1A and Sar1B. We acknowledge support from the Office of Naval Research through the Oregon Nanoscience and Microtechnologies Institute, and the National Science Foundation (Award no. 1006171).

Appendix A. Supplementary data

Supplementary data associated with this article can be found, in the online version, at http://dx.doi.org/10.1016/j.bbrc.2012.08.131.

References

[1] H.T. McMahon, J.L. Gallop, Membrane curvature and mechanisms of dynamic cell membrane remodelling, Nature 438 (2005) 590–596.
[2] J. Zimmerberg, M.M. Kozlov, How proteins produce cellular membrane curvature, Nat. Rev. Mol. Cell Biol. 7 (2006) 9–19.
[3] R. Parthasarathy, J.T. Groves, Curvature and spatial organization in biological membranes, Soft Matter 3 (2007) 24–33.
[4] M. Huang, J.T. Weissman, S. Béraud-Dufour, P. Luan, C. Wang, W. Chen, et al., Crystal structure of Sar1-GDP at 1.7 Å resolution and the role of the NH2 terminus in ER export, J. Cell Biol. 155 (2001) 937–948.
[5] E.I. Settles, A.F. Loftus, A.N. McKeown, R. Parthasarathy, The vesicle trafficking protein Sar1 lowers lipid membrane rigidity, Biophys. J. 99 (2010) 1539–1545.
[6] K. Matsuoka, L. Orci, M. Amherdt, S.Y. Bednarek, S. Hamamoto, R. Schekman, et al., COPII-coated vesicle formation reconstituted with purified coat proteins and chemically defined liposomes, Cell 93 (1998) 263–275.
[7] M.C.S. Lee, L. Orci, S. Hamamoto, E. Futai, M. Ravazzola, R. Schekman, Sar1p N-terminal helix initiates membrane curvature and completes the fission of a COPII vesicle, Cell 122 (2005) 605–617.
[8] A. Bielli, C.J. Haney, G. Gabreski, S.C. Watkins, S.I. Bannykh, M. Aridor, Regulation of Sar1 NH2 terminus by GTP binding and hydrolysis promotes membrane deformation to control COPII vesicle fission, J. Cell Biol. 171 (2005) 919–924.
[9] M.C.S. Lee, E.A. Miller, Molecular mechanisms of COPII vesicle formation, Semin. Cell Dev. Biol. 18 (2007) 424–434.
[10] S.M. Stagg, C. Gurkan, D.M. Fowler, P. LaPointe, T.R. Foss, C.S. Potter, et al., Structure of the Sec13/31 COPII coat cage, Nature 439 (2006) 234–238.
[11] X. Bi, R.A. Corpina, J. Goldberg, Structure of the Sec23/24-Sar1 pre-budding complex of the COPII vesicle coat, Nature 419 (2002) 271–277.
[12] J. Wang, S. Dimov, W. Tempel, D. Yaniw, C. Arrowsmith, A. Edwards, et al., PDB ID: 2GAO (n.d.).
[13] B. Jones, E.L. Jones, S.A. Bonney, H.N. Patel, A.R. Mensenkamp, S. Eichenbaum-Voline, et al., Mutations in a Sar1 GTPase of COPII vesicles are associated with lipid absorption disorders, Nat. Genet. 34 (2003) 29–31.
[14] J.C. Fromme, L. Orci, R. Schekman, Coordination of COPII vesicle trafficking by Sec23, Trends Cell Biol. 18 (2008) 330–336.
[15] C. Barlowe, R. Schekman, SEC12 encodes a guanine-nucleotide-exchange factor essential for transport vesicle budding from the ER, Nature 365 (1993) 347–349.
[16] R. Parthasarathy, Rapid, accurate particle tracking by calculation of radial symmetry centers, Nat Methods, 2012.
[17] S.K. Sainis, V. Germain, E.R. Dufresne, Statistics of particle trajectories at short time intervals reveal fN-scale colloidal forces, Phys. Rev. Lett. 99 (2007) 018303.
[18] D. Axelrod, D.E. Koppel, J. Schlessinger, E. Elson, W.W. Webb, Mobility measurement by analysis of fluorescence photobleaching recovery kinetics, Biophys. J. 16 (1976) 1055–1069.
[19] C.W. Harland, D. Rabuka, C.R. Bertozzi, R. Parthasarathy, The *M. tuberculosis* virulence factor trehalose dimycolate imparts desiccation resistance to model mycobacterial membranes, Biophys. J. 94 (2008) 4718–4724.
[20] D. Axelrod, D.E. Koppel, J. Schlessinger, E. Elson, W.W. Webb, Mobility measurement by analysis of fluorescence photobleaching recovery kinetics, Biophys. J. 16 (1976) 1055–1069.
[21] C.W. Harland, Z. Botyanszki, D. Rabuka, C.R. Bertozzi, R. Parthasarathy, Synthetic trehalose glycolipids confer desiccation resistance to supported lipid monolayers, Langmuir 25 (2009) 5193–5198.
[22] C.W. Harland, D. Rabuka, C.R. Bertozzi, R. Parthasarathy, The *Mycobacterium Tuberculosis* virulence factor trehalose dimycolate imparts desiccation resistance to model Mycobacterial membranes, Biophys. J. 94 (2008) 4718–4724.
[23] Y.-H. Wang, A. Collins, L. Guo, K.B. Smith-Dupont, F. Gai, T. Svitkina, et al., Divalent cation-induced cluster formation by polyphosphoinositides in model membranes, J. Am. Chem. Soc. 134 (2012) 3387–3395.
[24] N. Richnau, Å. Fransson, K. Farsad, P. Aspenström, RICH-1 has a BIN/Amphiphysin/Rvsp domain responsible for binding to membrane lipids and tubulation of liposomes, Biochem. Biophys. Res. Commun. 320 (2004) 1034–1042.
[25] B.J. Peter, H.M. Kent, I.G. Mills, Y. Vallis, P.J.G. Butler, P.R. Evans, et al., Bar domains as sensors of membrane curvature: the amphiphysin bar structure, Science 303 (2004) 495–499.
[26] L. Mrówczyńska, C. Lindqvist, A. Iglič, H. Hägerstrand, Spontaneous curvature of ganglioside GM1 – Effect of cross-linking, Biochem. Biophys. Res. Commun. 422 (2012) 776–779.
[27] E. Strandberg, D. Tiltak, S. Ehni, P. Wadhwani, A.S. Ulrich, Lipid shape is a key factor for membrane interactions of amphipathic helical peptides, Biochimica Et Biophysica Acta (BBA) – Biomembranes 1818 (2012) 1764–1776.
[28] J. Liu, Y. Sun, G.F. Oster, D.G. Drubin, Mechanochemical crosstalk during endocytic vesicle formation, Curr. Opin. Cell Biol. 22 (2010) 36–43.